Heliyon 10 (2024) e26679

Contents lists available at ScienceDirect

Heliyon

journal homepage: www.cell.com/heliyon

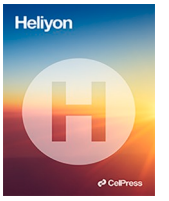

Research article

In-plane compressive responses and failure behaviors of composite sandwich plates with resin reinforced foam core

Zhiwen Qin [a,b,*,1], Xiaofei Song [c,1], Caicai Liao [a,b], Lu Yu [a,b], Xin Liu [a,b], Shu Yan [a,b], Xinkai Li [a,b,**]

[a] Offshore Wind Energy Department, Huaneng Clean Energy Research Institute, Beijing, 102209, China
[b] Research and Development Center of National Energy Offshore Wind Power Engineering and Operation Technology, Beijing, 102209, China
[c] School of Energy and Power Engineering, Inner Mongolia University of Technology, Hohhot, 010051, China

ARTICLE INFO

Keywords:
Sandwich structure
Core machining configuration
Core thickness
In-plane compressive
Failure load
Failure mode

ABSTRACT

The paper presented an experimental study on the effect of the resin reinforced core configuration and core thickness on in-plane compressive responses and failure behaviors of composite sandwich specimens. Two resin reinforced core machining configurations were designed with three core thickness along. In-plane compressive load, displacement, strains on both sides, and failure morphology were closely monitored during the loading process. Meanwhile, the theoretical method also was supplementary to forecast the failures of sandwich structures. It was found that the enhancement of grooved, perforated holes and contour cut (GPC) core was better than double-side grooved and perforated hole (DGP) core to improve the in-plane compressive capacity of sandwich specimens for all thick cores. The core fracture or skin/core debonding failure of sandwich specimens resulted in an instant drop of in-plane compressive load, and the global buckling led to a slower reduction. The failure mode changed from global buckling to skin/core debonding at both sides as the core thickness increased for the Plain core sandwich specimen; switched from global buckling to a combined failure of core fracture and skin/core debonding at both sides, and then to skin/core debonding at both sides for the DGP core sandwich specimen; the skin/core debonding at the shallow side occurred for all GPC core specimens. The slight buckling trace of strains before the peak load probably triggered the skin/core debonding of sandwich specimens. The theoretical method could well forecast failure loads and corresponding failure modes of sandwich specimens with the 15 mm thick core, and reasonably predict failure loads for sandwich specimens with 30 mm and 45 mm thick cores.

1. Introduction

The composite sandwich structure consists of two thin outer skins of high stiffness and high strength and a thicker core material in the middle, which has many advantages such as high specific strength, high specific stiffness, superior designability and economy, etc. It is widely used in the fields of aerospace, transportation, energy, and construction [1–5]. Compared with honeycomb, Balsa wood,

* Corresponding author. Offshore Wind Energy Department, Huaneng Clean Energy Research Institute, Beijing, 102209, China.
** Corresponding author. Offshore Wind Energy Department, Huaneng Clean Energy Research Institute, Beijing, 102209, China.
E-mail addresses: zw_qin@qny.chng.com.cn (Z. Qin), xk_li2@qny.chng.com.cn (X. Li).
[1] These authors contributed equally to this work.

https://doi.org/10.1016/j.heliyon.2024.e26679
Received 18 November 2023; Received in revised form 4 February 2024; Accepted 17 February 2024
Available online 21 February 2024

aluminum foam, and grid core, polymer foam core has the advantages of low density and low cost, so it is used in a larger proportion of sandwich structures [6,7]. However, low-density pure foams often fail to meet the design requirements due to insufficient mechanical properties or excessive material usage. Improving the mechanical properties of the core material through appropriate reinforcement on the foam core is an alternative way to achieve low-cost lightweight structures.

Currently, there are several popular strategies to strengthen foam sandwich structures such as Z-pin technique [8–11], stitching technique [12–15], lattice ribs reinforcement [16–19], and core machining method [20–27], etc. The Z-pin technique is to improve the mechanical properties of the sandwich structures by embedding metal or fibrous rods into sandwich composites to form a spatial grid structure. The Z-pin technique has a large improvement in the compression and shear performance of the reinforced foam core sandwich structures compared to the traditional pure foam core sandwich structures [11]. The stitching technique uses fiber lines to stitch the skins and core layer of sandwich structures, making the mechanical properties of the core and sandwich structure significantly improved in the through-thickness direction. The stitching technique can solve the problem of weak skin/core interface of traditional sandwich structures, and therefore can significantly improve the flat compressive, out-of-plane shear, and bending performance [14,15]. Space lattice ribs reinforced cores is another way to strengthen composite sandwich structures, the bending stiffness, strength, and energy absorption of sandwich structure can be greatly improved through proper design of the materials and space distribution of lattice ribs [16,19]. Another method is to use mechanical processing to generate grooves and perforations in the core layer, which will be filled with high-performance resin, and therefore enhancing the mechanical properties of the foam core and sandwich structures [27].

Truxel et al. [20] investigated the skin/core interface resistance to the debonding of composite sandwich structures with five machining configurations in the core layer. Sandwich plate tilt debonding test were conducted to investigate the skin/core interface resistance. The results reveal that transverse resin grooves can effectively inhibit the rapid growth of cracks and wide grooves are more effective in inhibiting crack expansion. May-Pat et al. [21] tested the in-plane compressive and shear performance of composite sandwich structures with through-thickness holes in cores and found that the compression and shear moduli of sandwich structures obtain a significant increase. Mitra et al. [22] innovatively proposed a semi-circular cross-section epoxy shear bond based on composite sandwich structures and found that the delamination resistance of the new sandwich structure are improved by about 25%. Fathi et al. [23] investigated the bending performance of composite sandwich structures with different core machining configurations in core layer, the results showed that contour cut substantially enhances the shear strength and bending stiffness of the sandwich structures. Yalkin et al. [25] designed through-thickness hole and glass fiber sewn sandwich structure specimens, and found that through-thickness hole can moderately improve the mechanical properties of the sandwich structure, and sewing can improve the mechanical properties more significantly and increase the weight less. The resin-filled holes and resin-impregnated fiber columns can effectively prevent the deformation of the foam, thus reducing the bending deflection and shear strain at failure. The performance of the skin/core interface has also been the focus of many scholars. Qin et al. [27] designed composite sandwich specimens with three core machining configurations and the test specimens prepared by vacuum assisted resin infusion (VARI) process are subjected to static tensile, compression, shear, and peel tests according to ASTM standards. The compression and shear strengths are significantly improved.

The above enhancement methods are mainly concerned with improving the properties of the sandwich structure such as tensile, bending, out-of-plane compression and shear, and skin/core bond strength along the through-thickness direction. The in-plane compression is also an important load component for sandwich structures, such as naval ships, spacecraft, wind turbine blades, etc.

As to in-plane compressive responses and failure behaviors of composite sandwich structures, some researchers have conducted inspiring studies. Phan et al. [28] conducted theoretical predictions and tests for in-plane compression of composite sandwich plates and found that the predictions of extended high-order sandwich plate theory are closest to the experimental The results show that the theory can be used to predict the critical load of the non-uniform honeycomb core sandwich structure. Tao et al. [29] used composite stiffeners to prevent skin wrinkling of sandwich structures, Results indicate that the failure mode of sandwich composite structures with stiffeners transferred from skin wrinkling to compressive micro-buckling or global buckling, and the average ultimate load and specific strength were substantially improved compared to sandwich composites without stiffeners. Boccaccio et al. [30] used the corrugation projection method to measure the deformation and monitor the buckling behavior during compression tests, the results show that increasing the relative thickness of the core material can prevent buckling from occurring. Japins et al. [31] conducted quasi-static in-plane compression tests on composite sandwich plates to investigate the effects of the plate thickness, layup, core density, and other factors on the failure behavior of the sandwich structure during in-plane compression and found that the main failure modes are skin crush and skin wrinkling. Fleck et al. [3] found that the highest failure load is for the short sandwich plate with the highest density. The failure modes of sandwich specimens are mainly caused by Euler buckling, core shear buckling, and skin wrinkling, the difference between these failure modes is mainly determined by the geometry and material of the sandwich structures. Eyvazian et al. [32] obtained various failure modes such as skin/core debonding, core fracture, Euler buckling, and plate wrinkling occurred by changing the specimen slenderness ratio, skin material, foam core structure, end support conditions, etc. The results reveal that failure modes and the failure load are affected by the material properties and geometry. Lei et al. [33] found that the critical failure load decreases significantly with the increase of length, and the first- and second-order buckling modes play a dominant role in the failure process through failure morphology observation.

Although the in-plane compression performance of sandwich structures has attracted the attention of some researchers, the influence of the geometry and reinforced strategy of the sandwich core on its in-plane compression strength and failure behaviors has not been fully discussed, and the failure mode of sandwich plates that appears as competing mechanisms can affect the critical failure loads [33], which should be fully considered when predicting the failure load of sandwich plates. On the other hand, it is rare to investigate the in-plane compressive responses of sandwich plates with core machining configurations, and the reinforced resin configurations

directly affect the interfacial properties and core properties of sandwich structures, which inevitably affect the in-plane compression properties of sandwich structures, so it is significant to analyze and summarize the effects of core geometry and core machining configurations on the in-plane compression properties of sandwich structures and their failure behaviors.

In this study, two patterns of resin reinforced cores were designed, and composite sandwich specimens were prepared by the VARI process. Theoretical predictions were compared with experimental results, and the effects of core thickness and core machining configurations on the ultimate load capacity and failure behaviors of sandwich structures were investigated.

2. Experiments

2.1. Specimen preparation

The foam selected for the present study is the polyurethane foam provided by NMG COMPOSITES Co., Ltd. (Jiaxing, China), and the corresponding density is about 0.123 g/cm^3. The mechanical properties of HPE110 foam are shown in Table 1. The resin (LT-5078A) and corresponding curing agent (LT-5078B-3) used in this study are provided by Huibai New Material Technology Co., Ltd. (Shanghai, China), and the mass ratio of epoxy resin to curing agent is 100:30 ± 1, the density of the epoxy resin after 70 °C × 8h curing is about 1.137 g/cm^3, and the mechanical properties of the cured resin are from the manufacture, as shown in Table 2.

The glass fiber LTX1200 used is triaxial non-woven glass fabric provided by NMG COMPOSITES Co., Ltd, and the corresponding areal mass in three directions (0°/45°/-45°) are 709 g/m^2, 251 g/m^2, 251 g/m^2, respectively. The mechanical properties of the composite material (LTX1200/LT-5078) composed of LTX1200 glass fabric and LT-5078A/LT-5078B-3 epoxy resin are shown in Table 3.

The subscripts 1 and 2 align with the 0° and 90° directions of the glass fibers (see Table 3). The subscripts *t*, *c*, and *s* stand for the tension, compression, and shear strength. Therefore, E_1, E_2, G_{12}, U_{ts}, U_{cs}, and U_{ss} represent the elastic moduli in 0° and 90° directions, the in-plane shear modulus, the tensile and compressive strengths in the 0° direction, and the in-plane shear strength, respectively.

The composite sandwich plates were fabricated by the VARI process, which is popularly used for manufacturing large thin-wall composite structures due to its low cost, porosity, and environmental hazards. The procedure of the VARI process for manufacturing composite sandwich plates was operated as follows. Firstly, the glass fibric, core material, glass fibric, peel ply, perforated release film, and resin redistribution medium were laid on the operating desk, and then sealed by vacuum bag and sealant to form a mold cavity. Secondly, one side of the sandwich plate was connected to the vacuum pump by a plastic pipe to pump out the air sealed in the vacuum bag and to form a lower pressure. Meanwhile, the opposite side of the sandwich plate was connected to the resin bracket, the resin was infused into the inner of the vacuum bag under the pressure difference between the atmosphere and the inner vacuum bag.

The lay-ups of the sandwich structure and the auxiliary material for the VARI process are shown in Fig. 1(a). The vacuum pressure produced through the vacuum pump was set at −0.1 MPa. Fig. 1(b) shows a moment of the infusing process for the sandwich plate, it can be seen that the groove can speed the resin infusion in the sandwich structure that the resin flowed ahead in the grooves of the core, when the flow front arrived at the side of the extraction port, the resin import should be carefully observed to avoid the resin being sucked into the vacuum pump. For a 500 mm × 500 mm sandwich plate, about 12 min were needed to fully infuse into the plate. The sandwich plates were cured by heating for 8 h at 70 °C. After curing, the plates were demolded and machined to the required dimensions using a high-speed cutting machine to obtain the expected specimens.

2.2. Core machining configuration design

Three types of foam core machining configurations were designed: flat (Plain) core, double-side grooved and perforated hole (DGP) core, and grooved, perforated holes and contour cut (GPC) core. Where Plain core is a foam board without any processing, DGP core is based on Plain core with shallow criss-cross grooves on both sides and perforated holes at the intersections, and GPC core is based on DGP core with shallow criss-cross grooves on one side, perforations, and narrower deep criss-cross grooves on the other side, as shown in Fig. 2. The geometrical dimensions of core machining configurations were shown in Table 4.

2.3. Test methods and apparatuses

In order to investigate the effect of geometrical parameters and core machining configuration on the in-plane compressive performance and failure modes of composite sandwich structure, specimens were prepared and tested according to ASTM C364-07 standard [34]. The universal material testing machine is MTS CMT 5205. As shown in Fig. 3, the real-time strain in the loading direction was obtained during the test by strain gauges pasted on the geometric center of the outer surface of both sides of specimens. The real-time displacement and corresponding load of the specimen were also recorded during the test. The loading rate was 1 mm/min,

Table 1
Mechanical properties of HPE110 foam core.

Typical performance	Compressive strength (MPa)	Compressive modulus (MPa)	Tensile strength (MPa)	Tensile modulus (MPa)	Shear strength (MPa)	Shear modulus (MPa)
HPE110	1.1	60	1.1	55	0.95	20

Table 2
Mechanical properties of the cured epoxy resin LT-5078A/LT-5078B-3.

Mechanical properties	Value
Tensile modulus (MPa)	65–75
Tensile modulus (MPa)	2800–3500
Elongation at break (%)	≥5

Table 3
Mechanical properties of LTX1200/LT-5078.

E_1 (GPa)	E_2 (GPa)	G_{12} (GPa)	U_{ts} (MPa)	U_{cs} (MPa)	U_{ss} (MPa)
32.9	14.5	8.48	706	726	209

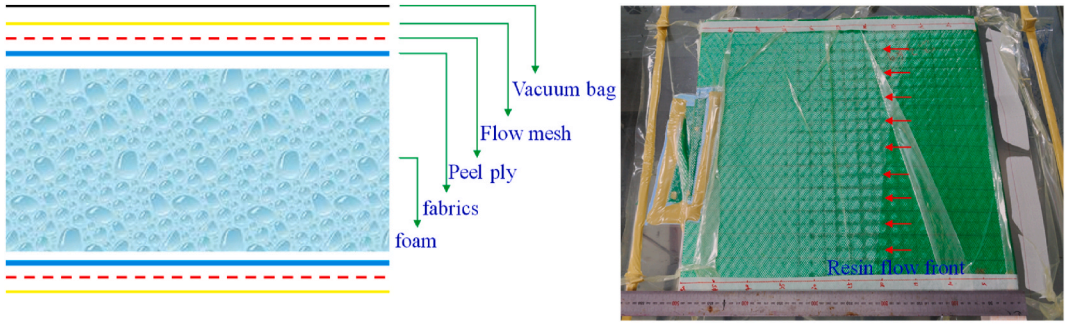

Fig. 1. Specimen fabrication: (a) schematic diagram of sandwich structure lay-ups and auxiliary materials and (b) a moment of resin flow in the sandwich plate.

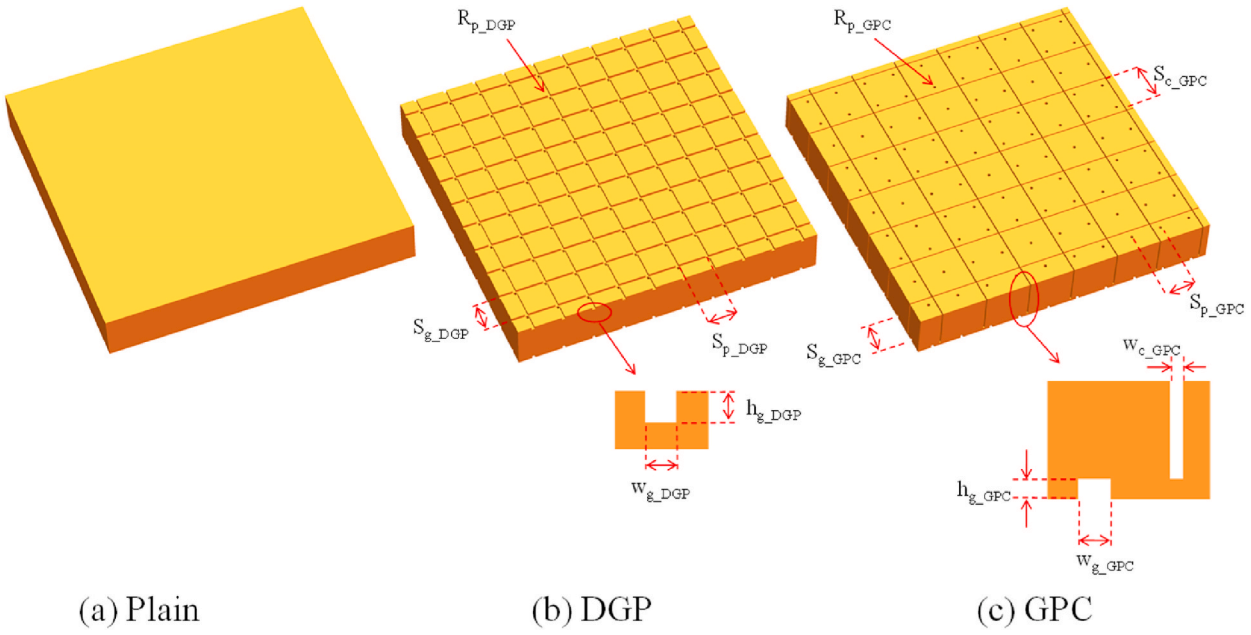

Fig. 2. Core machining configurations.

Table 4
Geometric dimensions and spacings of core machining configurations.

Nomenclature	Shallow groove spacing of DGP S_{g_DGP}	Shallow groove depth of DGP h_{g_DGP}	Width of shallow groove of DGP w_{g_DGP}	Hole spacing of DGP S_{p_DGP}	Hole radius of DGP R_{p_DGP}		
Value/mm	20 × 20	2.0	2.0	20 × 20	1.0		
Nomenclature	Shallow groove spacing of GPC S_{g_GPC}	Shallow groove depth of GPC h_{g_GPC}	Width of shallow groove of GPC w_{g_GPC}	Hole spacing of GPC S_{p_GPC}	Hole radius of GPC R_{p_GPC}	Deep groove spacing of GPC S_{c_GPC}	Deep groove width of GPC w_{c_GPC}
Value/mm	20 × 20	2.0	2.0	20 × 20	1.0	30 × 30	0.8

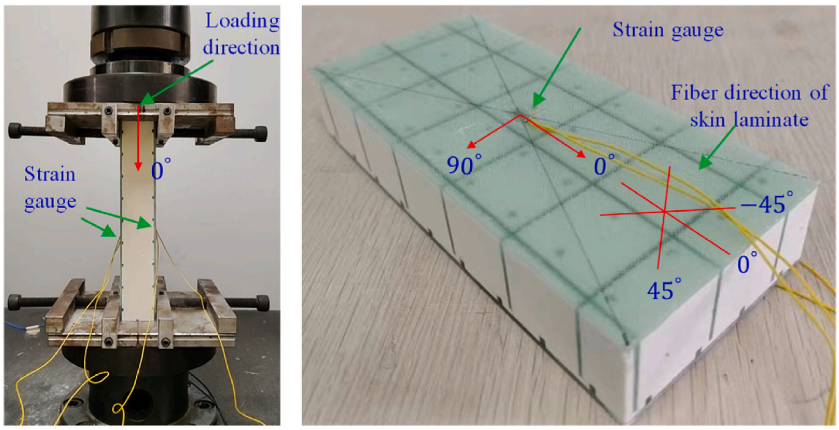

Fig. 3. Test specimen and apparatus: (a) specimen fixed on the test machine and (b) locations of strain gauges.

and the behavior of the specimen during the whole loading process was continuously captured by video.

2.4. Specimen design

Nine groups of specimens were designed with a least five valid specimens in each group. The lay-ups and thicknesses of the upper and lower skins of all sandwich specimens are the same. The core thicknesses of 15 mm, 30 mm, and 45 mm and core machining configurations of the Plain, DGP, and GPC cores were considered in the study. The design of specimen groups is shown in Table 5 specimen length, specimen width, upper (or lower) skin thickness, and core thickness as shown in Fig. 4, and the design dimensions of the specimens are shown in Table 5.

3. Theoretical model

In-plane compression is one of the most important forms of loading for sandwich structures [35], The complexity of the material and structure determines that in-plane compression failure of the sandwich structure is determined by a variety of competing failure mechanisms, such as Euler buckling, core shearing, skin fracture, skin wrinkling, and skin/core debonding [32].

Table 5
Specimen design.

Specimen group No.	Skin lay-up	Core thickness (mm)	Foam specification	Core machining configuration	Specimen length (mm)
#1	$[0/45/-45]_2$	15	HPE110	Plain	180
#2				DGP	
#3				GPC	
#4		30		Plain	
#5				DGP	
#6				GPC	
#7		45		Plain	
#8				DGP	
#9				GPC	

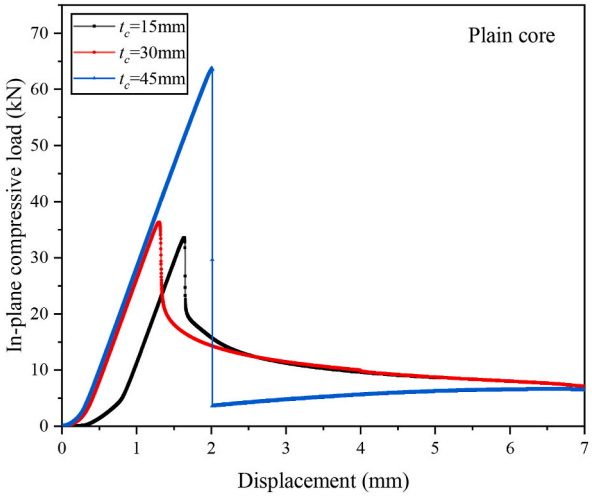

Fig. 4. Load-displacement curves of Plain core sandwich specimens.

3.1. Global buckling

Global buckling is one of the most common failure modes of sandwich structures. The presence of transverse shear can significantly reduce the global buckling critical load of sandwich structures, so it should not be neglected when predicting the global buckling. The method to consider the effect of transverse shear in the prediction process of global buckling of the sandwich structure is most widely applied by the Engesser method [36], and the critical load P_{cr} is given by equation (1):

$$P_{cr} = \frac{P_E}{1 + \beta P_E / (AG_{eq})}, \tag{1}$$

$$P_E = \frac{\pi^2 (EI)_{eq}}{(\mu L)^2}. \tag{2}$$

Where P_E is the Euler buckling load, derived from equation (2); μ is the length factor, whose value depends on the rotational freedom of the end of the specimen [37,38], μ is equal to 0.5 for clamped constraint on both ends; L is the effective length; $(EI)_{eq}$ is the equivalent bending stiffness, which is derived from equation (3) [33]:

$$(EI)_{eq} = \frac{b}{6} E_s t_s^3 + \frac{b}{2} E_s t_s d^2 + \frac{b}{12} E_c {t_c}^3. \tag{3}$$

For sandwich structures with thin skin, the sectional equivalent shear modulus is basically equal to the core shear modulus, and β is the shear correction factor, determined by equation (4):

$$\frac{\beta}{AG_{eq}} = \frac{1}{b(t_c + t_s)G_c}. \tag{4}$$

Substituting equation (4) into equation (1) to obtain the overall flexural expression as shown in equation (5) [39]:

$$\frac{1}{P_{cr}} = \frac{1}{P_E} + \frac{1}{AG_c}, \tag{5}$$

$$A = b(t_c + t_s). \tag{6}$$

Where b denotes the width of the specimen, d denotes the distance between the two geometric centers of sandwich skins, t_s and t_c denote the thickness of the skin and core material of sandwich specimens, respectively, and E_s and E_c denote the moduli of elasticity of the skin and core material, respectively. According to equation (5), the global buckling load is mainly determined by the core shear stiffness when the core shear modulus of the sandwich structure is very small, and conversely the global buckling load depends on the Euler buckling failure.

3.2. Skin wrinkling

The skin wrinkling belongs to the local buckling, for sandwich structures with the thin skin and light-weight core, the skin wrinkling is also an important failure mode, the wavelength of its buckling mode is of the same order of magnitude as the core

thickness, the short wave instability of sandwich structures compared to Euler buckling often occurs with a very small load and shows a smaller load carrying capacity after failure. Some scholars have empirically concluded that t_s/t_c is less than a certain constant value as the condition for local buckling to start controlling the failure of the sandwich structure, but it is difficult to be promoted by material limitations.

Skin wrinkling can be classified into symmetric wrinkling and antisymmetric wrinkling according to the mode of wrinkling. According to Hoff and Mautner's formulas [40], all types of critical wrinkling stresses can be calculated from equation (7) as follows:

$$\sigma_{Cr-Wrinkling} = \frac{1}{2}(E_s E_c G_c)^{1/3}. \tag{7}$$

The critical wrinkling load of sandwich specimens can be calculated from equation (8) [29]:

$$P_{Cr-Wrinkling} = 2bt_s\sigma_{Cr-Wrinkling} = bt_s(E_s E_c G_c)^{1/3}. \tag{8}$$

3.3. Skin crush

Here it is considered that the critical failure load of sandwich specimens is the ultimate strength of the skin in the direction of compression, which is a relatively ideal way of failure, the so-called skin crush that the load reaches the limit of the bearing capacity of the skin leading to crushing and fracture. Assuming the thickness of both skins is equal, the crush load of both skins can be calculated by the following equation [41]:

$$P_{Skin-Crush} = 2A_s\sigma_s. \tag{9}$$

Here, A_s denotes the cross-sectional area of the skin and σ_s is the ultimate compressive strength of the skin.

4. Results and discussion

4.1. The effect of core thickness on the in-plane compressive responses and failure behaviors

4.1.1. Plain core machining configuration

Fig. 4 depicts load-displacement curves of Plain core sandwich specimens with 15 mm, 30 mm, and 45 mm thick cores (the specimen with the failure load closest to the average failure load of the group was selected in each group). The load increased nearly linearly with displacement to the peak load and then decreased sharply to a smaller value for each specimen. The loads of sandwich specimens with 15 mm and 30 mm thick cores dropped slowly after a sharp drop to 20 kN, while the load of the sandwich specimen with the 45 mm thick core increased slowly after a sharp drop to about 5 kN.

Fig. 5 illustrates typical failure modes of Plain core sandwich specimens. From Fig. 5(a), it can be seen that the sandwich specimen with the 15 mm thick core exhibited core shear deformation in the lower and middle part of the specimen indicating a global buckling failure mode; the sandwich specimen with the 30 mm thick core exhibited global bending deformation indicating global buckling failure mode, as shown in Fig. 5(b), no visible skin/core debonding phenomenon was observed in sandwich specimens with 15 mm and 30 mm thick cores because no apparent sounds were heard. The sandwich specimen with the 45 mm thick core exhibited skin/core debonding with a loud sound, as shown in Fig. 5(c), which occurred instantaneously when the load reached the critical value. Compared with the shear buckling and Euler buckling failure modes of sandwich specimens with 15 mm and 30 mm thick cores, the debonding failure process of sandwich specimens with the 45 mm thick core experienced a shorter time deformation, as confirmed by the trend of the load-displacement curves shown in Fig. 4, that the load dropped from the peak load to a very small value with on change in displacement.

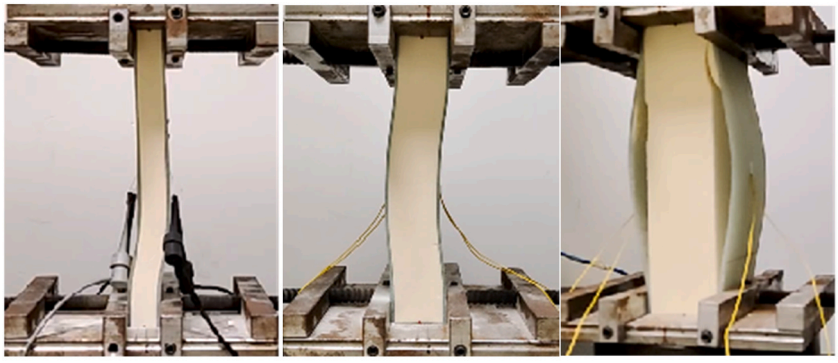

Fig. 5. Failure modes of Plain core sandwich specimens: (a) t_c = 15 mm, (b) t_c = 30 mm, and (c) t_c = 45 mm.

Fig. 6 shows load-strain curves of Plain core sandwich specimens with 15 mm, 30 mm, and 45 mm thick cores, it can be seen that strains on both sides of sandwich specimens increased approximately linearly with applied loads to the respective peak load for all three specimens. For sandwich specimens with 15 mm and 30 mm thick cores, strains on one side of sandwich specimens increased and the other side decreased when further loading after each peak load point, as shown in Fig. 6(a) and (b), which indicated that buckling mode of sandwich specimens occurred at the moment. This inference also was correlated with the observed buckling failure modes shown in Fig. 5(a) and (b). For the sandwich specimen with the 45 mm thick core, the strains on both sides increased continuously when further loading after each peak load point.

Fig. 7 shows failure loads and corresponding failure modes of Plain core sandwich specimens. Where the green bars represented experimental failure loads and observed failure modes, and the red bars represented analytical failure loads and corresponding failure modes according to the classical theory in Section 3. From the figure it can be seen that the failure load increased with the core thickness of sandwich specimens, which indicated that the in-plane compressive load carrying capacity of sandwich specimens was strengthened by thickening the inner core.

At the same time, the analytical method can well predict the failure load and corresponding failure mode when the core thickness of Plain core sandwich specimens was equal to 15 mm. While the analytical method could roughly predict the failure load, and could not predict the corresponding failure mode when the core thickness of Plain core sandwich specimens was equal to 30 mm and 45 mm. The test failure loads of Plain core sandwich specimens with 30 mm and 45 mm thick cores were slightly lower and higher than their theoretical failure loads, respectively. According to the analytical method stated in Section 3, the preferential failure mode of Plain core sandwich specimens with 30 mm and 45 mm thick cores was skin wrinkling, but the observed failure modes mainly were global buckling and skin/core debonding, respectively.

4.1.2. DGP core machining configuration

Fig. 8 shows the load-displacement curves of DGP core sandwich specimens with 15 mm, 30 mm, and 45 mm thick cores. Similar to the Plain core sandwich specimens, the loads ascended approximately linearly with displacements to their maximum loads and then decreased sharply to smaller values for all specimens, and then the values maintained for a long while with a small change.

Fig. 9 exhibits the photographs of failure modes of DGP core sandwich specimens with 15 mm, 30 mm, and 45 mm thick cores. The DGP sandwich specimen with the 15 mm thick core showed the failure of global buckling; while the DGP core sandwich specimen with

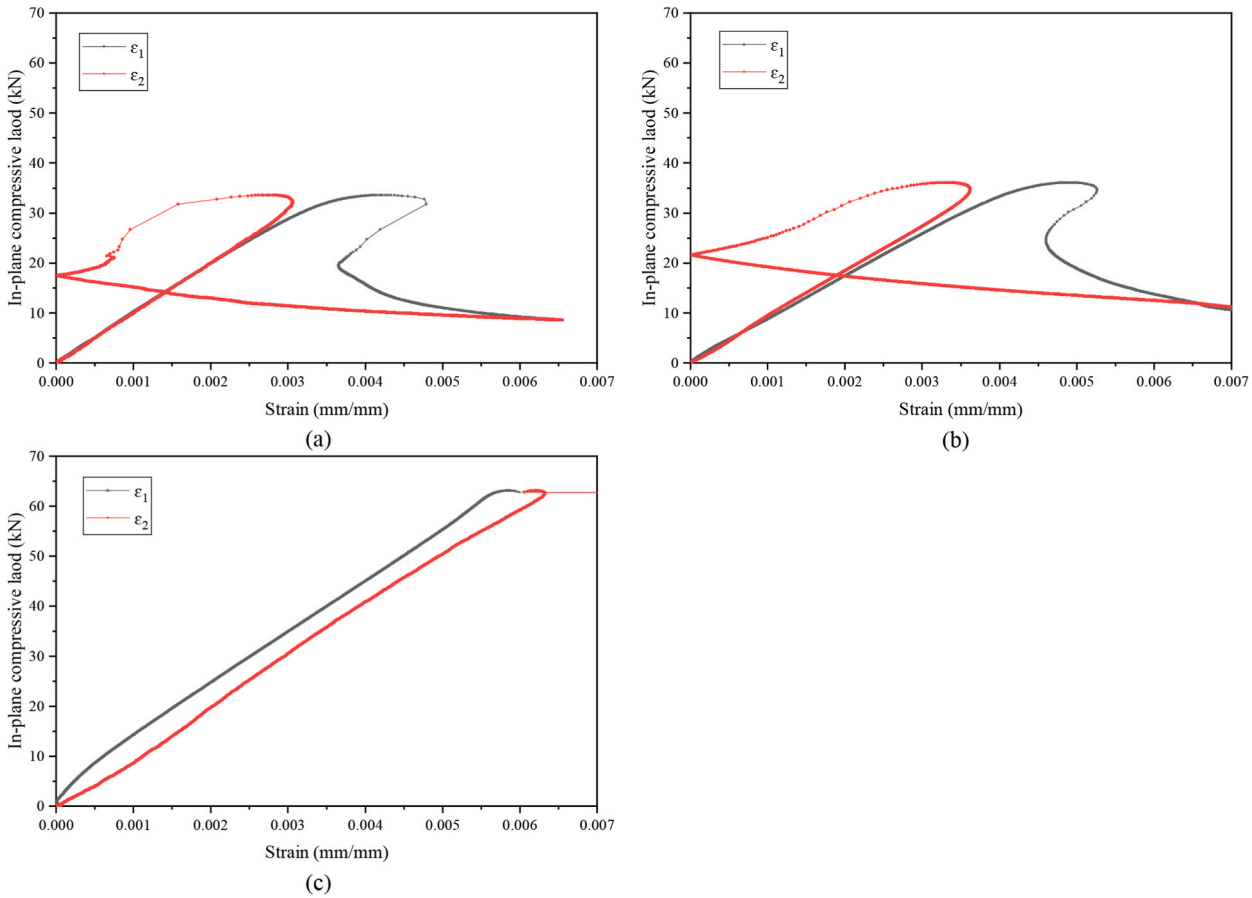

Fig. 6. Load-strain curves of Plain core sandwich specimens: (a) $t_c = 15$ mm, (b) $t_c = 30$ mm, and (c) $t_c = 45$ mm.

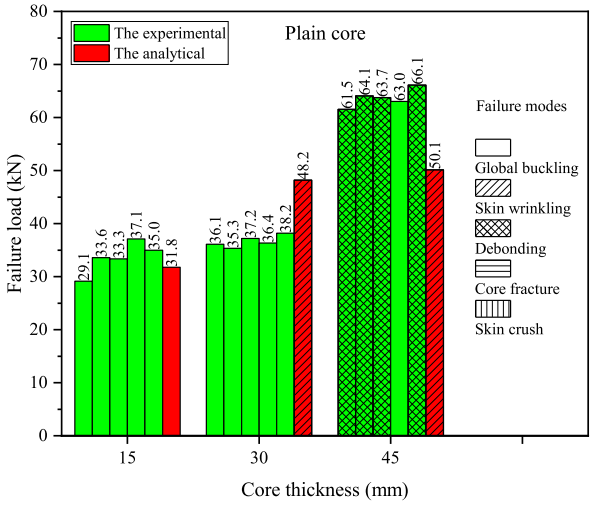

Fig. 7. Failure loads and corresponding failure modes of Plain core sandwich specimens.

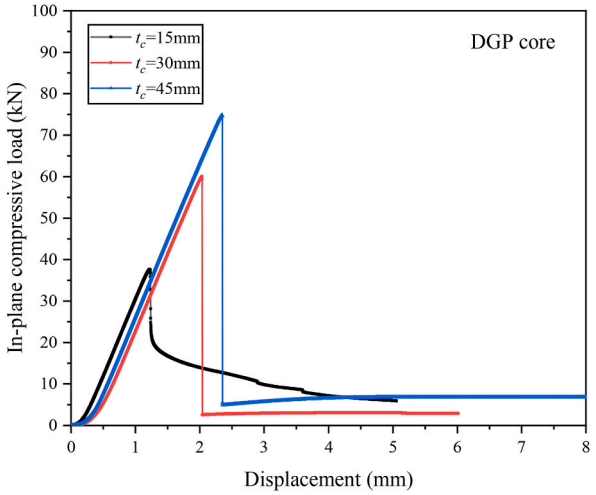

Fig. 8. Load-displacement curves of DGP core sandwich specimens.

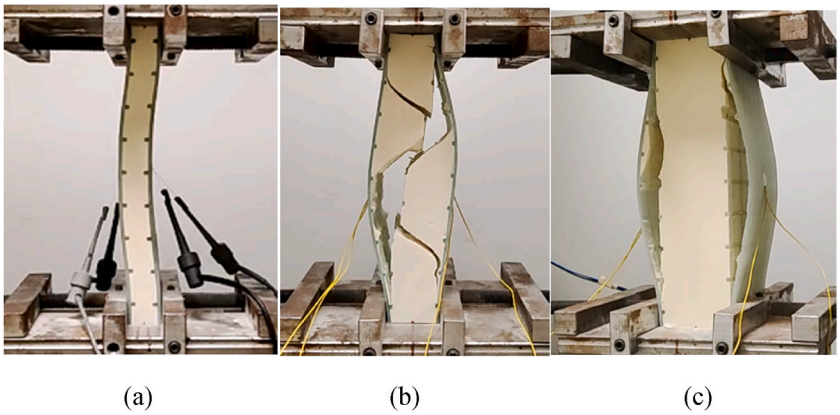

Fig. 9. Failure modes of DGP core sandwich specimens: (a) t_c = 15 mm, (b) t_c = 30 mm, and (c) t_c = 45 mm.

the 30 mm thick core manifested a combination failure of core fracture and skin/core debonding, and the DGP core sandwich specimen with the 45 mm thick core showed skin/core debonding failure at both sides.

Fig. 10 shows strain curves of sandwich specimens with applied load. As can be seen from Fig. 10(a), strains on both sides of the DGP core sandwich specimen with the 15 mm thick core approximately linearly increased with the applied load, when the load approached the maximum value, the strain on one side of the sandwich specimen increased while the strain on the other side decreased, and the specimen presented an obvious buckling signal, this was also confirmed by the test observation as shown in Fig. 9 (a).

It can be seen from Fig. 10(b) and (c) that strains on both sides of DGP core sandwich specimens with 30 mm and 40 mm thick cores roughly linearly increased as the load increased, when loads of DGP core sandwich specimens approached their maximum values, the strain on one side increased slightly while the strain on the other side decreased slightly, which indicated slight buckling trace.

Fig. 11 shows failure loads and corresponding failure modes of DGP core sandwich specimens. The failure loads of sandwich specimens ascended with the increase of the core thickness. The in-plane compressive strength can be improved through increasing the core thickness.

As can be seen that the theoretical method can well predict the failure load and the corresponding failure mode of sandwich specimens with the 15 mm thick core. Meanwhile, the theoretical method can well predict the loads of sandwich specimens with 30 mm and 45 mm thick cores, and could not predict the failure modes for 30 mm and 45 mm thick core specimens.

4.1.3. GPC core machining configuration

Fig. 12 depicts load-displacement curves of GPC core sandwich specimens with 15 mm, 30 mm, and 45 mm thick cores. Similar to Figs. 4 and 8 for Plain and DGP core sandwich specimens, the loads also increased approximately linearly with displacement to the peak load and then decreased sharply to smaller values for all specimens, all sandwich specimens experienced a sharp decrease in load carrying capacity after the failure load. The failure occurrence was accompanied with a short and loud rupture sound.

Fig. 13 illustrates typical failure modes of GPC core sandwich specimens. From the figure as can be seen that the sandwich specimen with the 15 mm thick core apparently exhibited a coupling failure of global buckling and partly skin/core debonding, and the two failure modes occurred almost simultaneously. Sandwich specimens with 30 mm and 45 mm thick cores presented skin/core debonding at the shallow groove side. The asymmetric debonding behavior can be explained by the asymmetric core reinforcement, the deep groove of the core was filled with a large amount of resin to improve the strength and made the core less susceptible to failure, while the shallow groove side was the weak region to break initially because there was not enough resin reinforcement.

Fig. 14 displays load-strain curves of GPC core sandwich specimens with 15 mm and 30 mm thick cores. Unfortunately, the strain data of the sandwich specimen with the 45 mm thick core was not properly saved during the test due to careless handling. The in-plane compressive load increased roughly linearly with strains on both sides of sandwich specimens with 15 mm and 30 mm thick cores, the strain on one side of the sandwich specimen with the 15 mm thick core soared dramatically and the strain on the other side dropped dramatically when the in-plane compressive load exceeded the peak load, the classical nonlinear change of strains did not occur, in combination of Fig. 12 that sharp drop of load-displacement of the GPC core sandwich specimen with the 15 mm thick core, it can be concluded that skin/core debonding was the initial failure and happened before global buckling of the sandwich specimen. Meanwhile, the strain on one side of the sandwich specimen with the 30 mm thick core increased slightly and the strain on the other side decreased slightly when the in-plane compressive load surpassed the peak load, slight bucking trace was also observed in the specimen similar to Figs. 6(c) and 10(c).

Fig. 15 illustrates failure loads and corresponding failure modes of GPC core sandwich specimens. The failure load of the sandwich specimen increased with the increase of the core thickness.

From the figure as can be seen that the theoretical method can reasonably predict the failure load and the corresponding failure mode of sandwich specimens with the 15 mm thick core. However, the theoretical method overestimated failure loads, and could not predict the failure modes of sandwich specimens with 30 mm and 45 mm thick cores. Where the observed failure mode was skin/core debonding compared with the predicted skin wrinkling.

4.2. Discussion

4.2.1. Ultimate load capacity

As can be seen from Figs. 7, 11 and 15, the ultimate in-plane compressive capacity increased with the increase of core thickness for Plain, DGP, and GPC core sandwich specimens, respectively. A similar finding also was obtained by Ref. [30] that the in-plane compressive capacity increases with the increase of core thickness. For sandwich specimens with identical thick core, the ultimate in-plane compressive capacity of the GPC core sandwich specimen was higher than that of the DGP core sandwich specimen; and the ultimate in-plane compressive capacity of the DGP core sandwich specimen was higher than that of the Plain core sandwich specimen.

4.2.2. Failure behaviors and modes

From load-displacement diagrams (shown in Figs. 4, Figure 8, and Fig. 12) and failure mode diagrams (shown in Figs. 5, Figure 9, and Fig. 13) of sandwich specimens, it can be concluded that the in-plane compressive load of the sandwich specimen would greatly decrease instantly when the core fracture or skin/core debonding occurred. However, when global buckling occurred, the in-plane compressive load of the sandwich specimen decreased slowly after an obvious decrease with the further increase of buckling deformation.

For Plain core sandwich specimens, the failure mode varied from global buckling to skin/core debonding at both sides as the core

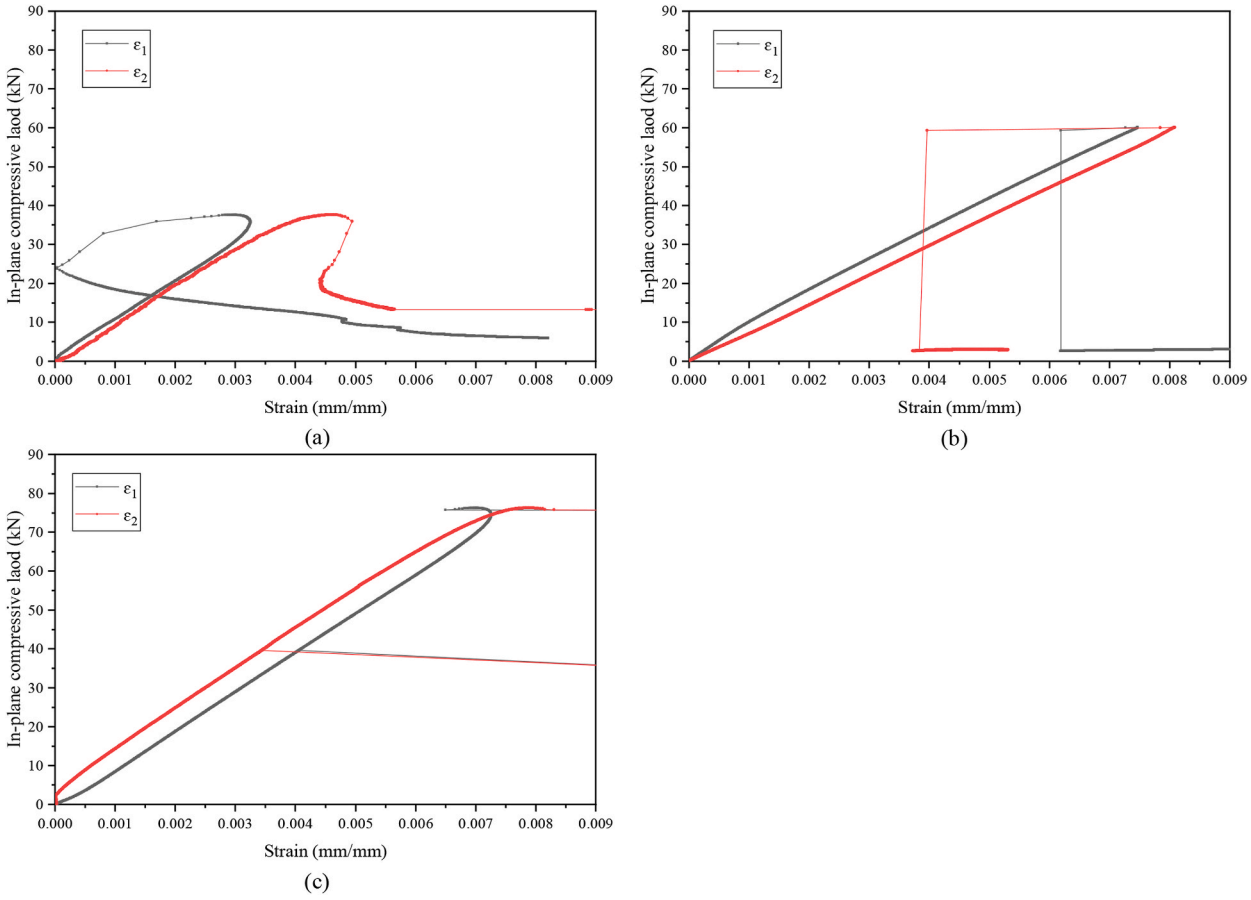

Fig. 10. Strain curves of DGP core sandwich specimens: (a) t_c = 15 mm, (b) t_c = 30 mm, and (c) t_c = 45 mm.

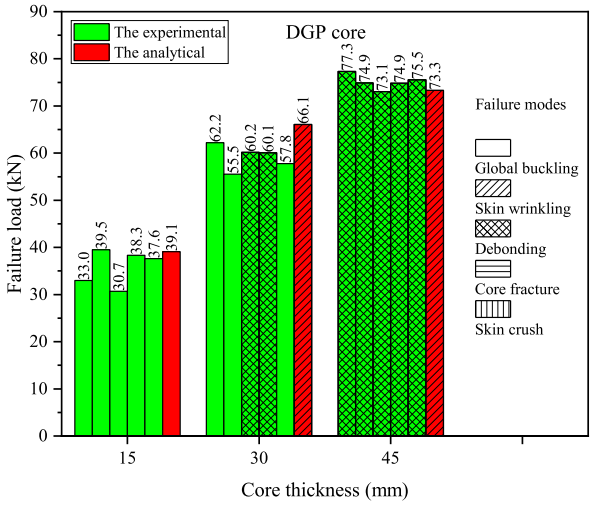

Fig. 11. Failure loads and corresponding failure modes of DGP core sandwich specimens.

thickness increased. For DGP core sandwich specimens, the failure mode changed from global buckling to a combined failure of core fracture and skin/core debonding at both sides, and then to skin/core debonding at both sides with the increase of the core thickness, Fleck et al. [3] also found similar failure modes of Euler buckling, core shear buckling, and skin wrinkling are likely to happen for the sandwich specimen without core reinforcement. For GPC core sandwich specimens, the failure of all specimens occurred with

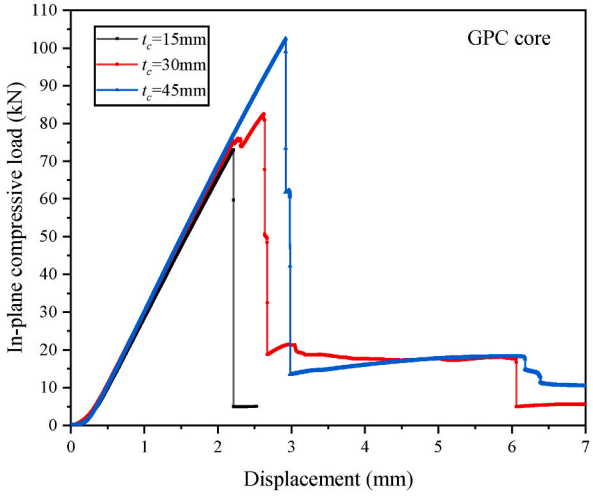

Fig. 12. Load-displacement curves of GPC core sandwich specimens.

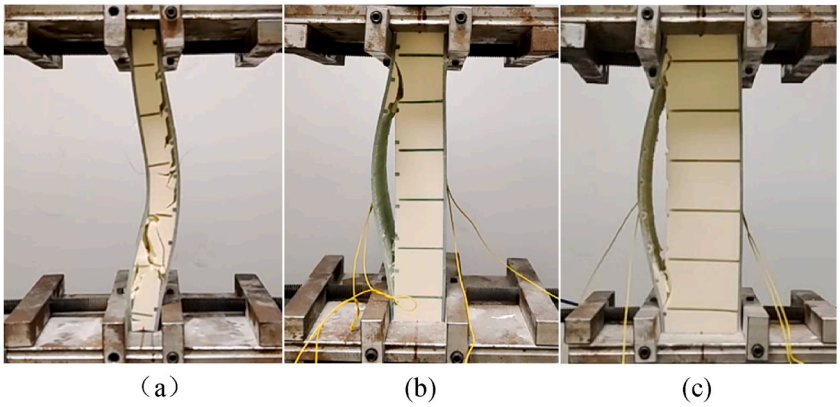

Fig. 13. Failure modes of GPC core sandwich specimens: (a) t_c = 15 mm, (b) t_c = 30 mm, and (c) t_c = 45 mm.

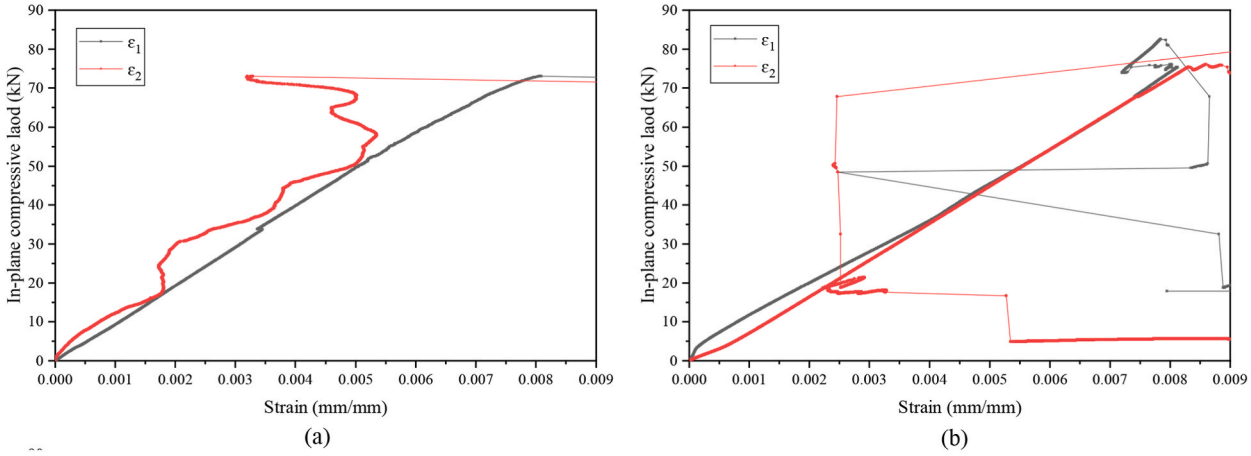

Fig. 14. Load-strain curves of GPC core sandwich specimens: (a) t_c = 15 mm, (b) t_c = 30 mm, and (c) t_c = 45 mm.

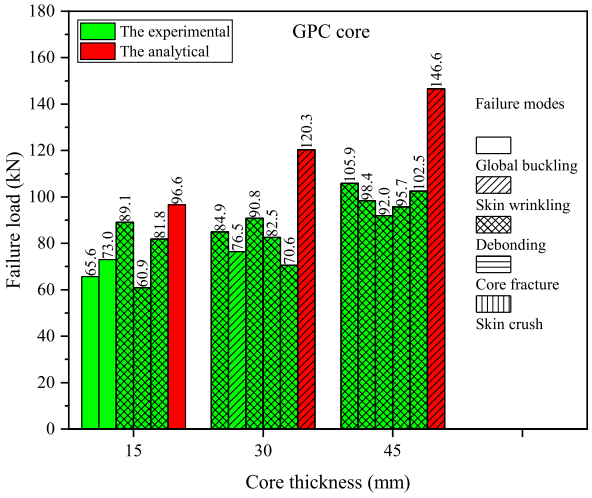

Fig. 15. Failure loads and corresponding failure modes of GPC core sandwich specimens.

skin/core debonding at the shallow side, Qin et al. [27] also found the shallow side of sandwich specimens is weaker than the other side in the shear test.

From failure mode diagrams (shown in Figs. 5, Figure 9, and Fig. 13) and strain curves (shown in Figs. 6, Figure 10, and Fig. 14) of sandwich specimens, it can be concluded that skin/core debonding of most sandwich specimens occurred after a slight buckling trace that strains on both sides experienced a short while of bifurcation, it can be deduced that specimen buckling probably triggered the skin/core debonding.

4.2.3. Prediction accuracy of analytical method

From experimental and theoretical failure loads and corresponding failure modes of sandwich specimens, shown in Figs. 7, 11 and 15. From these figures as can be seen that the classical analytical method can well predict failure loads and corresponding failure modes of sandwich specimens with the 15 mm thick core, while most specimens exhibited global buckling. When the core thickness was 30 mm, the predicted failure loads of sandwich specimens were very close to their experimental values. For sandwich specimens with the 45 mm thick core, the difference between the predicted and test failure loads was larger than that of 30 mm thick core sandwich specimens, respectively.

From strain curves and failure modes monitored in the tests, it was found that the skin/core debonding of sandwich specimens often occurred after a tiny buckling deformation, and the buckling deformation could be considered as a disturbance leading to skin/core debonding. Compared with global buckling, skin wrinkling, known as local buckling, theoretically happens along with a buckling deformation with a smaller wavelength. This evidence indicated that there was a close relationship between skin/core debonding and skin wrinkling of sandwich specimens, but it was still not easy to judge whether the final failure mode of observed skin/core debonding phenomenon represented the occurrence of skin wrinkling based on current experiment data.

5. Conclusions

In-plane compression is the dominating load for many large thin-wall sandwich composites. Two configurations of resin reinforced cores were designed, and three thickness cores were considered in order to improve the bearing capacity of the composite sandwich structure and clarify the influence of resin reinforced configuration on its performance. The in-plane compressive responses and failure behaviors of sandwich specimens were experimentally studied. Meanwhile, analytical methods were implemented to predict the failure in comparison with test results. The following conclusions were reached.

The ultimate in-plane compressive capacity of sandwich specimens with all three cores increased with the increase of core thickness. The ultimate in-plane compressive capacity of the GPC core sandwich specimen was higher than that of the DGP core sandwich specimen for the specimens with the identical thick core, and the DGP core sandwich specimen was higher than that of the Plain core.

The in-plane compressive load of the sandwich specimen greatly decreased instantly after peak load when the core fracture or skin/core debonding occurred, while decreased slowly when global buckling occurred.

The failure mode changed from global buckling to skin/core debonding at both sides as the core thickness increased for Plain core sandwich specimens; switch from global buckling to a combined failure of core fracture and skin/core debonding at both sides, and then to skin/core debonding at both sides for DGP core sandwich specimens; The skin/core debonding at the shallow side occurred for all GPC core specimens, accompanied with global buckling for the sandwich specimen with the 15 mm thick core. Skin/core debonding of most sandwich specimens occurred after a slight buckling trace, which probably triggered the skin/core debonding.

The classical analytical method could well predict failure loads and corresponding failure modes of sandwich specimens with the

15 mm thick core and roughly predict failure loads for sandwich specimens with 30 mm and 45 mm thick cores.

In this paper, the influence of core thickness and resin reinforced configuration on the in-plane compression performance of sandwich composites was studied. However, the skin wrinkling was not clearly found in the experiment in comparison with analytical results which theoretically should occurred. There was no reliable analytical method to predict the skin/core debonding occurred in the experiment, this will be the work to be further studied.

Data availability statement

The authors declare that the data supporting the findings of this study are available within the paper, a request for more detailed data should be sent to the corresponding authors with the permission of all authors.

CRediT authorship contribution statement

Zhiwen Qin: Writing – original draft, Writing – review & editing, Methodology, Investigation, Formal analysis, Conceptualization. **Xiaofei Song:** Writing – original draft, Writing – review & editing, Software, Methodology, Investigation, Formal analysis. **Caicai Liao:** Writing – review & editing, Software. **Lu Yu:** Writing – review & editing. **Xin Liu:** Resources, Formal analysis. **Shu Yan:** Resources, Formal analysis. **Xinkai Li:** Resources, Investigation.

Declaration of competing interest

The authors declare that there is no known competing financial interests or personal relationships that could have appeared to influence the work reported in this paper.

Acknowledgements

the authors gratefully acknowledge the financial support from National Key Research and Development Program of China (No. 2022YFE0207000) and (No. 2022YFB4201300), and China Huaneng Group Science and Technology Project (No. HNKJ20-H54). We are also grateful to Dr. Yu Zhengrong for his revisions on wording and phrasing, and the anonymous reviewers for their insightful comments and valuable suggestions for improving this paper.

References

[1] Q. Ma, et al., A review of the recent trends on core structures and impact response of sandwich panels, J. Compos. Mater. 55 (18) (2021) 2513–2555.
[2] V. Birman, G.A. Kardomateas, Review of current trends in research and applications of sandwich structures, Compos. B Eng. 142 (2018) 221–240.
[3] N.A. Fleck, I. Sridhar, End compression of sandwich columns, Compos. Appl. Sci. Manuf. 33 (3) (2002) 353–359.
[4] D.R. Veazie, K.R. Robinson, K. Shivakumar, Effects of the marine environment on the interfacial fracture toughness of PVC core sandwich composites, Compos. B Eng. 35 (6) (2004) 461–466.
[5] D.D. Luong, D. Pinisetty, N. Gupta, Compressive properties of closed-cell polyvinyl chloride foams at low and high strain rates: experimental investigation and critical review of state of the art, Compos. B Eng. 44 (1) (2013) 403–416.
[6] J. Xiong, et al., Mechanical behavior and failure of composite pyramidal truss core sandwich columns, Compos. B Eng. 42 (4) (2011) 938–945.
[7] B. Yang, et al., Study on the low-velocity impact response and CAI behavior of foam-filled sandwich panels with hybrid facesheet, Compos. Struct. 132 (2015) 1129–1140.
[8] L. Du, J. Guiqiong, H. Tao, The elastic properties of sandwich structure with Z-pinned foam core, J. Reinforc. Plast. Compos. 28 (7) (2009) 813–831.
[9] A. Nanayakkara, S. Feih, A.P. Mouritz, Experimental analysis of the through-thickness compression properties of z-pinned sandwich composites, Compos. Appl. Sci. Manuf. 42 (11) (2011) 1673–1680.
[10] B. Abdi, et al., Flatwise compression and flexural behavior of foam core and polymer pin-reinforced foam core composite sandwich panels, Int. J. Mech. Sci. 88 (2014) 138–144.
[11] A.P. Mouritz, Review of z-pinned laminates and sandwich composites, Compos. Appl. Sci. Manuf. 139 (2020) 106128.
[12] P. Potluri, E. Kusak, T.Y. Reddy, Novel stitch-bonded sandwich composite structures, Compos. Struct. 59 (2) (2003) 251–259.
[13] B. Lascoup, et al., On the mechanical effect of stitch addition in sandwich panel, Compos. Sci. Technol. 66 (10) (2006) 1385–1398.
[14] F. Han, Y. Yan, J. Ma, Experimental study and progressive failure analysis of stitched foam-core sandwich composites subjected to low-velocity impact, Polym. Compos. 39 (3) (2018) 624–635.
[15] A. Shigang, et al., Effect of stitching angle on mechanical properties of stitched sandwich panels, Mater. Des. 50 (2013) 817–824.
[16] W. Liu, et al., Flexural performance of sandwich beams with lattice ribs and a functionally multilayered foam core, Compos. Struct. 152 (2016) 704–711.
[17] F. Zhang, et al., Flexural behavior of composite sandwich beams with different kinds of GFRP ribs in flatwise and edgewise positions, Compos. B Eng. 156 (2019) 229–239.
[18] F. Zhang, et al., Effect of shear span-to-depth ratio on the mechanical behavior of composite sandwich beams with GFRP ribs and balsa wood core materials, Thin-Walled Struct. 154 (2020) 106799.
[19] F. Zhang, et al., Mechanical properties of the composite sandwich structures with cold formed profiled steel plate and balsa wood core, Eng. Struct. 300 (2024) 117256.
[20] A. Truxel, et al., Influence of face/core interface on debond toughness of foam and balsa cored sandwich, J. Sandw. Struct. Mater. 8 (3) (2006) 237–258.
[21] A. May-Pat, F. Avilés, J.O. Aguilar, Mechanical properties of sandwich panels with perforated foam cores, J. Sandw. Struct. Mater. 13 (4) (2010) 427–444.
[22] N. Mitra, B.R. Raja, Improving delamination resistance capacity of sandwich composite columns with initial face/core debond, Compos. B Eng. 43 (3) (2012) 1604–1612.
[23] A. Fathi, et al., An investigation on the flexural properties of balsa and polymer foam core sandwich structures: influence of core type and contour finishing options, J. Sandw. Struct. Mater. 15 (5) (2013) 487–508.
[24] F.C. Stoll, Optimal design of sandwich core for wind turbine blade buckling resistance, in: 32nd ASME Wind Energy Symposium, American Institute of Aeronautics and Astronautics, Spartanburg, 2014, p. 175.
[25] H.E. Yalkin, B.M. Icten, T. Alpyildiz, Enhanced mechanical performance of foam core sandwich composites with through the thickness reinforced core, Compos. B Eng. 79 (2015) 383–391.

[26] M. Rosemeier, P. Buriticá, A. Antoniou, Impact of resin uptake of core materials on buckling of wind turbine blades, J. Phys. Conf. 1037 (4) (2018) 042001.
[27] Z. Qin, et al., The effects of core machining configurations on the mechanical properties of cores and sandwich structures, Materials 15 (2) (2022) 521.
[28] C.N. Phan, et al., Wrinkling of sandwich wide panels/beams based on the extended high-order sandwich panel theory: formulation, comparison with elasticity and experiments, Arch. Appl. Mech. 82 (10–11) (2012) 1585–1599.
[29] J. Tao, et al., In-plane compression properties of a novel foam core sandwich structure reinforced by stiffeners, J. Reinforc. Plast. Compos. 37 (2) (2017) 134–144.
[30] A. Boccaccio, et al., Structural response of polyethylene foam-Based sandwich panels subjected to edgewise compression, Materials 6 (10) (2013) 4545–4564.
[31] G. Japins, et al., Compressive failure of quasi-static indented CFRP/aluminium honeycomb sandwich panels, IOP Conf. Ser. Mater. Sci. Eng. 500 (1) (2019) 012007.
[32] A. Eyvazian, et al., Buckling and crushing behavior of foam-core hybrid composite sandwich columns under quasi-static edgewise compression, J. Sandw. Struct. Mater. 23 (7) (2019) 2643–2670.
[33] H. Lei, et al., Experimental and numerical investigation on the crushing behavior of sandwich composite under edgewise compression loading, Compos. B Eng. 94 (2016) 34–44.
[34] ASTMC364-07, *Standard Test Method for Edgewise Compressive Strength Ofsandwich Constructions*, American Society for Testing and Materials: American, 2012.
[35] N. Gupta Kishore, S. Sankaran, On the characterisation of syntactic foam core sandwich composites for compressive properties, J. Reinforc. Plast. Compos. 18 (14) (1999) 1347–1357.
[36] S.P. Timoshenko, J.M. Gere, W. Prager, Theory of Elastic Stability, second ed., 1962, p. 220, 29.
[37] B.-C. Lee, et al., The compressive response of new composite truss cores, Compos. B Eng. 43 (2) (2012) 317–324.
[38] R.G. Hutchinson, et al., Kagome plate structures for actuation, Int. J. Solid Struct. 40 (25) (2003) 6969–6980.
[39] H.G. Allen, Chapter 5 - bending and buckling of isotropic sandwich panels with very thin identical faces (ritz method), in: H.G. Allen (Ed.), Analysis and Design of Structural Sandwich Panels, Pergamon, 1969, pp. 76–98.
[40] N.J. Hoff, S.E. Mautner, The buckling of sandwich-type panels, J. Aeronaut. Sci. 12 (3) (1945) 285–297.
[41] H. Mathieson, A. Fam, Axial loading tests and simplified modeling of sandwich panels with GFRP skins and soft core at various slenderness ratios, J. Compos. Construct. 19 (2) (2015) 04014040.